Title
Observational evidence for the convective transport of dust over the Central United States

Journal
Journal of Geophysical Research: Atmospheres, 121(3)

ISSN
2169-897X

Authors
Corr, CA
Ziemba, LD
Scheuer, E
et al.

Publication Date
2016-02-16

DOI
10.1002/2015jd023789

AGU PUBLICATIONS

JGR

Journal of Geophysical Research: Atmospheres

RESEARCH ARTICLE
10.1002/2015JD023789

Special Section:
Deep Convective Clouds and Chemistry 2012 Studies (DC3)

Observational evidence for the convective transport of dust over the Central United States

C. A. Corr[1,2], L. D. Ziemba[3], E. Scheuer[1], B. E. Anderson[3], A. J. Beyersdorf[3], G. Chen[3], E. Crosbie[3,4], R. H. Moore[3], M. Shook[3,5], K. L. Thornhill[3,5], E. Winstead[3,5], R. P. Lawson[6], M. C. Barth[7], J. R. Schroeder[3,4], D. R. Blake[8], and J. E. Dibb[1]

[1]Earth Systems Research Center, Institute for the Study of Earth, Oceans, and Space, University of New Hampshire, Durham, New Hampshire, USA, [2]Now at NASA Postdoctoral Program, Chemistry and Dynamics Branch, NASA Langley Research Center, Hampton, Virginia, USA, [3]Chemistry and Dynamics Branch, National Aeronautics and Space Administration Langley Research Center, Hampton, Virginia, USA, [4]Oak Ridge Associated Universities, Oak Ridge, Tennessee, USA, [5]Science Systems and Applications Inc., Hampton, Virginia, USA, [6]SPEC Inc., Boulder, Colorado, USA, [7]National Center for Atmospheric Research, Boulder, Colorado, USA, [8]Department of Chemistry, University of California, Irvine, California, USA

Key Points:
- Dust transport through convection examined using aircraft observations
- Less than half of the inflow coarse dust removed by cloud processes
- Influence of ice particle shatter on observations appears minimal

Correspondence to:
C. A. Corr,
chelsea.a.corr@nasa.gov

Citation:
Corr, C. A., et al. (2016), Observational evidence for the convective transport of dust over the Central United States, *J. Geophys. Res. Atmos.*, *121*, 1306–1319, doi:10.1002/2015JD023789.

Received 11 JUN 2015
Accepted 13 JAN 2016
Accepted article online 14 JAN 2016
Published online 12 FEB 2016

Abstract Bulk aerosol composition and aerosol size distributions measured aboard the DC-8 aircraft during the Deep Convective Clouds and Chemistry Experiment mission in May/June 2012 were used to investigate the transport of mineral dust through nine storms encountered over Colorado and Oklahoma. Measurements made at low altitudes (<5 km mean sea level (MSL)) in the storm inflow region were compared to those made in cirrus anvils (altitude > 9 km MSL). Storm mean outflow Ca^{2+} mass concentrations and total coarse (1 μm < diameter < 5 μm) aerosol volume (V_c) were comparable to mean inflow values as demonstrated by average outflow/inflow ratios greater than 0.5. A positive relationship between Ca^{2+}, V_c, ice water content, and large (diameter > 50 μm) ice particle number concentrations was not evident; thus, the influence of ice shatter on these measurements was assumed small. Mean inflow aerosol number concentrations calculated over a diameter range (0.5 μm < diameter < 5.0 μm) relevant for proxy ice nuclei (N_{PIN}) were ~15–300 times higher than ice particle concentrations for all storms. Ratios of predicted interstitial N_{PIN} (calculated as the difference between inflow N_{PIN} and ice particle concentrations) and inflow N_{PIN} were consistent with those calculated for Ca^{2+} and V_c and indicated that on average less than 10% of the ingested N_{PIN} were activated as ice nuclei during anvil formation. Deep convection may therefore represent an efficient transport mechanism for dust to the upper troposphere where these particles can function as ice nuclei cirrus forming in situ.

1. Introduction

Mineral dust is one of the most abundant primary aerosols in the atmosphere, comprising over 30% of the aerosol mass for many areas [e.g., *Malm et al.*, 2004; *Querol et al.*, 2008; *Zhang et al.*, 2012]. In combination with its abundance, the optical, physical, and chemical properties make dust an important driver of climate and biogeochemical processes [e.g., *Jickells et al.*, 2005; *Benas et al.*, 2011; *Lui et al.*, 2012]. For instance, dust transported and deposited to remote ocean locations impacts ecosystems in those regions [e.g., *Jickells et al.*, 2005]. Atmospheric dust also directly scatters and absorbs radiation across the UV and visible spectrum thereby impacting climate and photochemistry [e.g., *Benas et al.*, 2011; *Fu et al.*, 2014].

Most recently, much work has focused on the indirect impact mineral dust can have on Earth's radiation budget through modification of cirrus cloud properties. Though cirrus cloud formation via homogeneous freezing is noted to occur under certain conditions [e.g., *Jensen et al.*, 2013; *Herbert et al.*, 2015], recent analyses of particle residual material have suggested heterogeneous freezing of dust contributes significantly to both anvil and synoptic cirrus formation [e.g., *Cziczo et al.*, 2013]. Numerous laboratory and in situ airborne measurements indicate mineral dust is a relatively efficient ice nuclei (IN) that initiates heterogeneous freezing processes at temperatures and relative humidities with respect to ice (RH_i) relevant to the upper troposphere [e.g., *DeMott et al.*, 2003a; *Koehler et al.*, 2007; *Kanji et al.*, 2011; *Hoose and Mohler*, 2012; *DeMott et al.*, 2015]. The heterogeneous freezing of dust at high altitudes impacts cirrus cloud formation primarily through the reduction of ice crystal number leading to an increase in the average size of the ice crystals [e.g., *DeMott et al.*, 2003a, 2003b; *Lohmann et al.*, 2008; *Lui et al.*, 2012]. These modifications reduce cirrus cloud radiative forcing relative to forcing from cirrus formed predominantly by homogeneous freezing, resulting in nonnegligible climate impacts [*Lohmann et al.*, 2008; *Lui et al.*, 2012].

Measurements of the composition of IN activated at cirrus temperatures in the free troposphere show large (diameters $> 0.5\ \mu m$) dust particles are common IN [*Richardson et al*., 2007; *DeMott et al*., 2010] and must therefore be available in upper troposphere where cirrus formation occurs. Modeling studies together with observations indicate deep convection is generally a good transport mechanism for both gases and aerosols, including dust, from the boundary layer to the upper troposphere [e.g., *Takemi et al*., 2006; *Engstrom et al*., 2008; *Froyd et al*., 2009; *Avery et al*., 2010; *Tulet et al*., 2010; *Seigel and Van den Heever*, 2012; *Yin et al*., 2012; *Fadnavis et al*., 2013; *Homeyer et al*., 2014]. For instance, modeled dust concentrations in high-altitude convective outflow regions (10–12 km) over a semiarid location were over twice the background concentrations for the same altitude range [*Yin et al*., 2012]. However, outflow concentrations were an order of magnitude smaller than those modeled for the inflow for the same study, suggesting dust ingested into convective systems is efficiently scavenged by cloud processes [*Yin et al*., 2012]. This is consistent with the findings of *Tulet et al*. [2010] who modeled a twofold decrease in dust concentrations for particles with diameters greater than $0.5\ \mu m$ when a parameterized scavenging scheme was incorporated into a modeled convective system.

In contrast, airborne measurements suggest convective systems may not efficiently scavenge dust [e.g., *Liang et al*., 2007; *Avery et al*., 2010]. Bulk aerosol measurements of calcium (Ca^{2+}) mass concentrations, a proxy for dust, in tropical outflow indicated, on average, ~50% of the inflow Ca^{2+} mass was transported through the sampled convective storms [*Avery et al*., 2010]. As bulk aerosol Ca^{2+} mass is typically associated with coarse-mode aerosol [e.g., *Kline et al*., 2004], elevated concentrations of Ca^{2+} mass in storm outflow suggests coarse dust is not scavenged efficiently contrary to the model results of *Tulet et al*. [2010]. While interpretations of outflow measurements in and near the storm anvil may be complicated by recently recognized measurement artifacts associated with ice particles [e.g., *Murphy et al*., 2004; *Jensen et al*., 2009; *Froyd et al*., 2010; *Korolev et al*., 2013; *Cziczo and Froyd*, 2014], elevated dust and dust tracer concentrations have also been seen in clear air at altitudes higher than those observed for synoptically lofted dust in the Saharan Air Layer (typically < 6 km) [e.g., *Prospero and Carlson*, 1972; *Tsamalis et al*., 2013]. For instance, elevated Ca^{2+} mass concentrations ($>0.17\ \mu g\ m^{-3}$) at altitudes greater than 8 km were observed over the Central U.S. [*Tabazadeh et al*., 1998; *Talbot et al*., 1998] as well as in an aged, cloud-free, Asian convective plume encountered off the U.S. Pacific Northwest coast [*Liang et al*., 2007].

The inconsistency between modeling results and observations regarding the presence of dust in convective outflow indicates that the transport mechanism of dust through convective systems is not well established. Given the potential impact of upper tropospheric dust on climate, a better understanding of the role of deep convection in vertical dust transport is necessary for accurate climate forecasting. Further, IN activation for mineral dust exhibits a strong size dependence with larger particles activating at higher temperatures and lower relative humidities with respect to ice than smaller particles [*DeMott et al*., 2010; *Koehler et al*., 2010]. Coarse-mode dust transported to high altitudes via deep convection could therefore have a greater impact on climate via cirrus cloud modification than smaller dust particles.

This work investigates the transport of coarse-mode dust through several storms encountered during the NSF-NASA Deep Convective Clouds and Chemistry Experiment (DC3) conducted in May/June 2012 [*Barth et al*., 2015]. Specifically, inflow and outflow bulk aerosol mass concentrations and particle size distribution measurements made aboard the NASA DC-8 aircraft were compared to assess the transport efficiency of coarse-mode dust through the storms. The possible influence of ice particle shattering on these aerosol measurements is discussed. Lastly, aerosol number concentrations for particles with diameters greater than $0.5\ \mu m$ in storm inflow were compared to measurements of ice particle concentrations in storm anvil cirrus to assess the likelihood of interstitial dust in the cirrus anvil.

2. Methods

2.1. DC3 Campaign

Twelve storms were surveyed in and around Colorado (CO) and Oklahoma (OK) by the DC-8 during DC3 in May/June 2012 (Table 1). As demonstrated by the example storm survey time series shown in Figure 1, inflow patterns were confined to altitudes less than ~5 km mean sea level (MSL) and often included vertical and horizontal components to characterize inflow regions during storm development. For fresh outflow, multiple level-leg passes across the anvil region ($9\ km < altitude < 12\ km$) were performed to characterize the evolution of the outflow composition with distance from the storm core.

Table 1. Name, Date, Inflow Times, Average Inflow Altitude, Outflow Times, and Average Outflow Altitude (Maximum and Minimum Altitude Values Are Shown in Parentheses) for All Storms of Interest During DC3[a]

Name	Flight Date	Inflow Times (UTC)	Inflow Altitude (km)	Outflow Times (UTC)	Outflow Altitude (km)
---	*18 May*	*22:10–22:52*	*3.93(1.52–5.41)*	*23:17–23:48*	*11.18(10.92–11.25)*
CO1	2 June	20:08–21:30	2.08(1.79–2.77)	21:58–23:09	11.23(10.41–12.03)
CO2	5 June	23:08–23:42	3.28(2.12–3.79)	0:03–0:38	9.50(9.18–10.18)
CO3	6 June	20:35–21:23	2.34(1.79–3.65)	21:47–21:57	10.80(10.43–11.21)
CO4	6 June	22:12–23:00	3.13(1.56–4.44)	23:27–23:52	11.48(11.08–12.30)
CO5	15 June	21:18–21:38	1.84(1.67–1.93)	22:13–22:36	10.98(10.06–11.19)
CO6	22 June	22:34–23:55	2.80(1.86–4.43)	0:16–1:39	10.81(9.08–11.30)
---	*19 May*	*22:35–0:14*	*3.06(1.23–5.41)*	*0:40–1:00*	*10.39(10.31–10.42)*
---	*25 May*	*23:42–0:54*	*3.04(1.25–4.85)*	*1:17–1:28*	*11.33(10.83–11.50)*
OK1	29 May	22:09–23:15	2.97(1.22–4.80)	23:40–0:13	10.48(9.77–11.12)
OK2	1 June	0:32–1:22	2.81(1.71–3.28)	1:38–2:00	11.17(11.09–11.89)
OK3	16 June	0:02–1:21	1.22(0.79–1.53)	1:41–2:02	11.84(11.71–11.86)

[a]IWC data that were not available for storms are in italics; thus, they were omitted from the analysis.

Here we focus on 9 of the 12 intercepted storms: 6 CO storms and three OK storms (Table 1). The other three storms (prior to 29 May) were excluded because ice water content (IWC) data were not available. Lightning is a known source of NO in the free troposphere [e.g., *Huntrieser et al.*, 1998; *Schumann and Huntrieser*, 2007]; therefore, time periods with NO concentrations higher than background values at outflow altitudes (>9 km MSL) were assumed to represent outflow measurements, whereas IWC in the outflow was taken as a marker for the cirrus anvil. High NO coincided with high IWC for all storms (e.g., Figure 1), suggesting storm outflow was limited to the anvil for the storms examined here. Therefore, only high-altitude survey times with IWC greater than 0 g m^{-3} were assumed to represent outflow periods for all storms.

Inflow regions were initially identified from the mission reports for each flight and were ultimately confirmed using video composites of DC-8 flight tracks and radar imagery. To focus the analysis on the transport of dust from the boundary layer, storm inflows were limited to flight times with altitude below cloud base height. Cloud base height was identified for each storm using profiles of temperature, dew point, and water vapor performed during storm surveys. Inflow analyses were also limited to altitudes above 0.5 km above ground level based on trajectory analysis by *Skamarock et al.* [2000] who showed air below this threshold was not necessarily ingested into convective systems. Identifying the inflow in this way introduces quantifiable variability into mean inflow values calculated from aerosol measurements as discussed below. Comparisons between mean aerosol volume size distributions calculated for discrete 0.1°×0.1° grid boxes within each inflow region and those calculated for the entire inflow area revealed no obvious spatial patterns within the inflow variability for any storms (Figure 2). Thus, the mean and standard deviations of aerosol properties calculated for storm inflow regions are assumed to be representative of the impacted region.

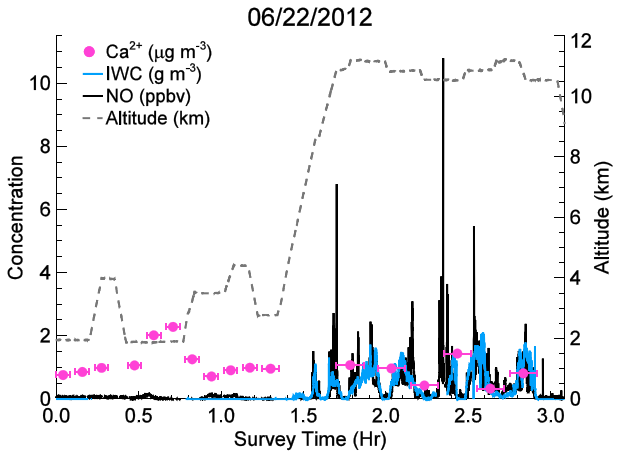

Figure 1. Time series of altitude (gray dashed line), NO (black solid line), IWC (blue solid line), and Ca^{2+} (pink circles) during the 22 June storm survey. Error bars on Ca^{2+} represent filter duration.

2.2. Measurements

Bulk aerosol mass composition was measured aboard the DC-8 during DC3 following the procedure and sampling setup outlined elsewhere [e.g., *Talbot et al.*, 1998; *Dibb et al.*, 2003; *McNaughton et al.*, 2007; *Thornhill et al.*, 2008]. Ambient sample was drawn into the sampling system through the University of New Hampshire (UNH) dual-sampling probe which consists of two leading edge diffuser inlets curved

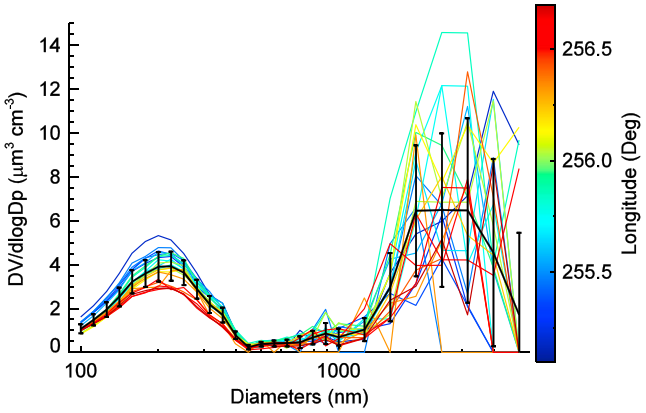

Figure 2. Mean volume size distributions calculated for $0.1 \times 0.1°$ boxes within the CO5 storm inflow region (color) and for the entire inflow region (black). Grid box mean volume size distributions are color coded by longitude. 1σ values for each size bin calculated for the entire inflow region are reported as error bars.

for isoaxial sampling. Each diffuser was encased in an anodized aluminum shroud, and flow rates were adjusted to maintain isokinetic sampling during level flight legs when bulk aerosol sampling occurs. Based on tests discussed by *McNaughton et al.* [2007], the sampling efficiency for this inlet is greater than 50% for particles with aerodynamic diameters smaller than 5 μm.

From the inlet, air was drawn through a 90 mm Teflon filter for variable time intervals which depend on both the length of the level leg as well as flight objectives (e.g., in plume versus background sampling). For DC3, inflow filters sampled for 5 min with the exception of one filter from OK1 which sampled for 7 min. Integration times for outflow filters ranged from 8 to 12 min though most (88%) of the filters used in this analysis had 10 min sampling periods. Such long integration times may complicate the comparison of inflow and outflow filter measurements. Given aircraft speeds greater than 110 m s^{-1} and the heterogeneity in the turbulent environment surrounding convective systems, the DC-8 aircraft likely sampled different air masses with variable amounts of aerosol, dilution, and entrainment over filter time periods. This is particularly true for outflow filters as outflow sampling consisted of both in-anvil and clear upper troposphere (UT) measurements. Despite this, on average, over 80% of each outflow filter time period was spend in regions with nonzero IWC, suggesting the aerosol concentrations reported for outflow filters are representative of aerosol in the convective outflow.

After sampling, filters were stored in clean room bags purged with zero air and placed in a cooler for postflight analysis. Postflight, water-soluble material was extracted from the filters using a small aliquot of ultrapure water; extracts were preserved using chloroform for later analysis at UNH. Preserved extracts were analyzed via ion chromatography (Dionex) for 10 ions: Na^+, NH_4^+, K^+, Mg^{2+}, Ca^{2+}, Cl^-, Br^-, NO_3^-, SO_4^{2-}, and $C_2O_4^{2-}$. Ion concentrations were corrected for filter artifacts using concentrations measured for filter blanks collected during each flight.

Additional online measurements of aerosol composition were made by the UNH mist chamber-ion chromatograph (MC/IC) system. Specifically, the MC/IC system reports submicron aerosol SO_4^{2-} mass concentrations. As described in *Scheuer et al.* [2010], sample is drawn into the sampling system via a short, window-mounted manifold. Ambient air subsampled from the manifold is drawn through a dense cloud of deionized water inside one of two glass mist chambers. Soluble gases and aerosol are removed and concentrated from the sampled air flow for approximately 85 s per sample interval. Because the mist chamber inlets are rear facing with respect to the manifold flow, aerosol particles with diameters greater than 1 μm are excluded [*Scheuer et al.*, 2010]. Constant sampling is achieved by alternating between two mist chambers.

Number size distributions between 100 and 5000 nm diameter were measured using a TSI 3340 Laser Aerosol Spectrometer (LAS). As with other optical particle sizing instruments, the LAS calculates particle size from the intensity of scattered light using Mie theory and calibrations performed using aerosol with a known size and refractive index [e.g., *Cai et al.*, 2011]. Specifically, ambient aerosol drawn into the LAS cavity scatters light produced by a Ne-He laser that is subsequently measured using an avalanche photodiode detector. The LAS was calibrated prior to and periodically during the DC3 mission using polystyrene latex spheres and thus is referenced to a real refractive index of 1.59. The accuracy of optical sizing probes such as the LAS depends on the referenced refractive index; thus, errors in dust size distributions can arise if the instrument is calibrated to a particle with a refractive index different from dust [*Ryder et al.*, 2013]. However, because this analysis relies on the comparison of LAS size distributions measured at low altitudes to LAS size distributions in the outflow,

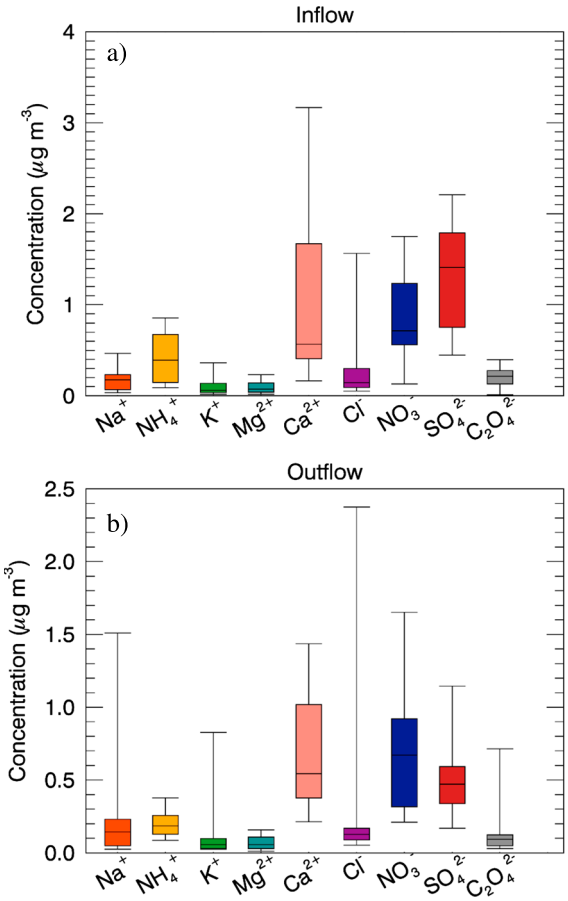

Figure 3. (a) Inflow and (b) outflow mass concentrations of bulk aerosol ions: Na^+ (orange), NH_4^+ (gold), K^+ (green), Mg^{2+} (teal), Ca^{2+} (coral), Cl^- (purple), NO_3^- (navy), SO_4^{2-} (red), and $C_2O_4^{2-}$ (gray). Box plots show median values (middle solid line), 50th percentile values (box outlines), and maximum and minimum values (whiskers) for all storms.

these errors are not expected to impact the analyses presented here. Number size distributions measured by the LAS at 1 Hz are used to calculate both aerosol number concentrations and volume size distributions (assuming spherical particles).

The LAS measured ambient air from the independent Langley Aerosol Research Group and University of Hawaii inlet, a window-mounted solid diffuser inlet which exhibits similar transmission efficiency to the UNH dual-sampling probe [*McNaughton et al.*, 2007]. Isokinetic flow through this solid diffuser inlet is maintained by manually adjusting the flow rate based on real-time air speed, static pressure, and temperature measurements [*Chen et al.*, 2011]. Air is dried to less than 40% RH using a Nafion dryer before measurement by the LAS, ensuring that size distributions are measured at the same RH regardless of sampling location (i.e., clear air versus in-cloud). Aerosol bulk composition and size data are reported in standard m^{-3} and standard cm^{-3}, respectively.

Ice particle size and concentration as well as IWC were determined based on images produced by the two-dimensional stereo (2D-S) probe mounted in a DC-8 wingtip pod during DC3. Modified tips and postprocessing algorithms using particle arrival times mitigate the effects of artifacts from ice particles shattering on the 2D-S probe [*Lawson*, 2011]. Additional information on the design and operation of the 2D-S and the postprocessing algorithms is provided in *Lawson et al.* [2006] and *Lawson* [2011].

Gas-phase measurements of nitric acid (HNO_3) and NO were used to identify storm scavenging and outflow, respectively. HNO_3 was measured using the MC/IC system described above. NO was measured using the NOAA airborne four-channel chemiluminescence instrument which is described in detail by *Ryerson et al.* [1999]. Potential disconnects between inflow and outflow air masses were identified using ratios of *n*-pentane to *i*-pentane. Both compounds were measured using the UC Irvine whole air sampler system (WAS) and gas chromatography; the details of WAS analyses for DC3 can be found in *Schroeder et al.* [2014]. Lastly, Particle Analysis by Laser Mass Spectrometry (PALMS) was used to determine single particle composition during DC3. Details of the PALMS technique have been provided elsewhere [e.g., *Murphy et al.*, 2006; *Froyd et al.*, 2009].

3. Results

Concentrations of all aerosol ions measured in both the inflow and outflow regions of the nine storms for which IWC data were available were highly variable as shown in Figure 3. Ranges in inflow bulk aerosol Ca^{2+} mass concentrations (0.16–3.17 μg m^{-3}) were particularly large, with generally higher concentrations at lower inflow altitudes (< ~2 km, see Figure 1). While variability in the filter blanks used to calculate mean blank correction values introduce some error into Ca^{2+} concentrations (±0.36 μg m^{-3} (1σ)), variability in Ca^{2+}

Table 2. Mean (1σ) Ca^{2+} Mass Concentrations, V_c, and *n*-Pentane/*i*-pentane Ratios for Storm Inflow and Outflow[a]

	Inflow			Outflow			Ratio	
	Ca^{2+} ($\mu g\ m^{-3}$)	V_c ($\mu m^3\ cm^{-3}$)	*n*-Pentane/*i*-pentane	Ca^{2+} ($\mu g\ m^{-3}$)	V_c ($\mu m^3\ cm^{-3}$)	*n*-Pentane/*i*-pentane	Ca^{2+}	V_c
CO1	0.39 (0.16)	2.20(5.65)	0.99(0.05)	0.58 (0.34)	1.21(5.07)	1.22[c](0.31)	1.50(1.09)	0.55(2.71)
CO2	N/A	2.55(6.84)	0.74(0.12)	BD	0.44(2.26)	1.07(0.03)	N/A	0.17(1.00)
CO3	0.46 (0.02)	2.02(5.19)	1.03(0.06)	0.43[b]	5.23(9.38)	BD	0.94(0.04)	2.59(8.10)
CO4	N/A	0.92(2.70)	0.89[b]	0.33 (0.07)	1.45(4.48)	1.09(0.04)	N/A	1.57(6.71)
CO5	N/A	4.02(6.97)	0.97[b]	0.60 (0.09)	5.02 (13.36)	0.91(0.04)	N/A	1.25(3.97)
CO6	1.44(0.68)	4.06(7.12)	0.93(0.06)	0.84 (0.42)	6.24 (13.33)	1.14[c](0.16)	0.58(0.40)	1.54(4.28)
OK1	1.73 (0.17)	2.22(5.34)	1.07(0.10)	0.71 (0.42)	1.89(5.45)	0.98[c] (0.04)	0.41(0.23)	0.85(3.21)
OK2	2.71 (0.64)	7.05(8.82)	0.96(0.03)	1.40 (0.05)	7.30 (13.72)	0.93[c](0.13)	0.52(0.12)	1.04(2.34)
OK3	0.45 (0.11)	0.86(2.74)	0.97(0.36)	0.372[b]	0.24(1.56)	0.99[c](0.06)	0.82(0.21)	0.28(2.02)

[a]Storms without Ca^{2+} or *n*-pentane/*i*-pentane ratios measured above detection limit are denoted as BD. Storms without filters that met inflow altitude criteria are denoted as N/A. Outflow/inflow ratios calculated using mean Ca^{2+} mass concentrations and V_c are also shown.
[b]Fewer than two samples.
[c]Outflow *n*-pentane/*i*-pentane statistically similar to inflow.

due to these errors is small compared to that observed for the inflow concentrations. The large ranges observed for inflow and outflow Ca^{2+} therefore likely reflect real temporal and vertical fluctuations in Ca^{2+} concentrations during storm surveys.

The variability in both inflow and outflow Ca^{2+}, together with the long sampling time periods needed for the filter measurements discussed above, introduces some uncertainty into the relationships between inflow and outflow air. Relying on inflow and outflow measurements from a single aircraft further complicates relationships between the inflow and outflow. As shown in Figure 1, sampling of storm outflow was delayed by at least 20 min following inflow sampling due to the time required for the aircraft to reach outflow altitudes. A simple calculation using the outflow sampling delays and the mean outflow and inflow altitudes for these storms suggests the DC-8 will only sample the same air parcel in the inflow and outflow for storms with updraft velocities less than 5 m s^{-1}. While convective systems in the study region are associated with median updraft velocities in this range, values greater than 10 m s^{-1} have also been frequently observed [*Giangrande et al.*, 2013]. Thus, some disconnect between inflow and outflow air is possible as a result of the limitations imposed by the filter measurements and sampling design.

To examine whether the inflow and outflow periods identified here were chemically similar, we use mean *n*-pentane to *i*-pentane ratios (Table 2). Only five of the nine storms have statistically similar ratios between inflow and outflow, suggesting the sources were different for the sampled inflow and outflow air masses. However, inflow Ca^{2+} concentrations are highly variable even for filters collected during these five storms as demonstrated by the mean and standard deviation of inflow Ca^{2+} (0.90 ± 0.89) that are nearly identical to those calculated for all storm filters (0.98 ± 0.84). This suggests the uncertainty in the measurements falls within the variability of Ca^{2+} and coarse aerosol in the inflow and outflow. We therefore conclude that qualitative comparisons between mean values calculated from inflow and outflow aerosol measurements still provide valuable insight into the transport efficiency of dust through the DC3 storms. Mean ratios for all storms are reported hereafter, recognizing that the large standard deviations of the means (due to natural variability) introduce similar uncertainty in the ratios (Table 2).

Mean inflow mass concentrations of Ca^{2+} were typically higher than mean outflow values as demonstrated by outflow/inflow Ca^{2+} ratios less than 1 for five of the six storms for which filter data were available (Table 2). The relatively large range in Ca^{2+} ratios (0.41–1.5) likely suggests dust transport efficiency through deep convection depends on individual storm characteristics (e.g., updraft velocity and precipitation rates). Moreover, as both updraft velocity and precipitation rates change with storm lifecycle stage, calculated transport efficiencies will vary depending on the stage at which sampling occurs. Despite this variability, outflow/inflow ratios for Ca^{2+} mass averaged for all storms (0.80) suggest that significant fractions of boundary layer dust can be transported through convective systems. Similar outflow/inflow mass ratios were observed for two other dust tracers, Mg^{2+} and K^+, as well as Na^+ and Cl^-, which are also likely associated with coarse-mode dust in this region [*Pratt et al.*, 2010] (Figure 4). In contrast, much smaller fractions of gas-phase HNO_3 (less than 0.1) and fine aerosol SO_4^{2-} (less than 0.3) remain in the outflow for all storms (not shown).

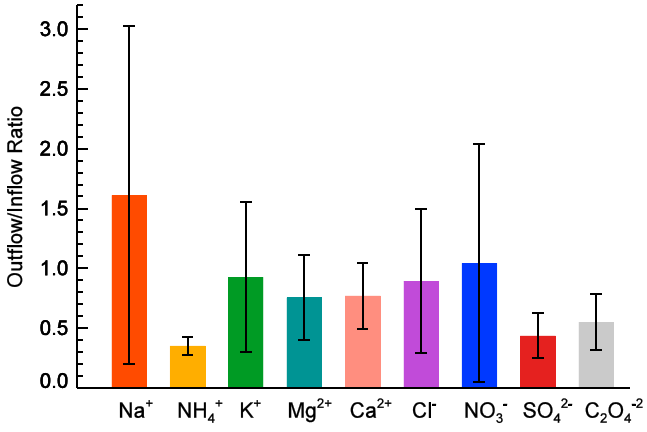

Figure 4. Mean outflow/inflow ratios for bulk aerosol ions: Na^+ (orange), NH_4^+ (gold), K^+ (green), Mg^{2+} (teal), Ca^{2+} (coral), Cl^- (purple), NO_3^- (blue), SO_4^{2-} (red), and $C_2O_4^{2-}$ (gray). Ratio error bars represent $\pm 1\sigma$.

Outflow/inflow ratios for bulk SO_4^{2-} were also lower than those determined for the dust tracers, though they were higher than the fine aerosol SO_4^{2-} ratios. This suggests that soluble gases and fine-mode aerosol were more readily removed than coarse aerosol during transport through the storms.

Decreases in the submicron mode between storm inflow and outflow were also observed in the average volume size distributions calculated for all storms (Figure 5). In contrast, the average outflow coarse (diameter $> 1\,\mu m$) volume size distribution is nearly equal to the mean inflow coarse volume size distribution. This is reflected in high total coarse-mode volume (V_c) in the outflow relative to the inflow for each storm (Table 2) calculated from volume size distributions using the equation

$$Vc = \sum_{D_p=1\ \mu m}^{D_p=5\ \mu m} \frac{dv}{d\log D_p} d\log D_p \quad (1)$$

where D_p is particle diameter. Calculations were limited to diameters between 1 and 5 μm given the inlet efficiencies discussed above. As shown in Table 2, outflow/inflow V_c ratios are high for nearly all storms, with five out of the nine exceeding unity. Such high ratios are surprising, particularly since some loss due to entrainment and/or dilution is expected. Mean ethane and CO outflow/inflow ratios calculated for all storms (0.64 ± 0.21 and 0.60 ± 0.15, respectively) [*Schroeder*, 2015] together with modeled entrainment rates for DC3 storms [*Barth et al.*, 2015; Fried et al., submitted manuscript, 2015] show that inflow air is diluted by ~40–60% as a result of entrainment and mixing in the outflow. As discussed below, sampling artifacts associated with sampling in ice clouds do not appear to influence the measurements discussed here. V_c and Ca^{2+} ratios greater than those reported for conservative gas-phase tracers therefore likely result from uncertainties associated with the filter sampling technique and design of the storm surveys discussed above. Additionally, the long-range transport of Asian plumes to the outflow regions of storms OK1 and OK3 [*Schroeder*, 2015] as well as a biomass burning plume observed in the OK1 and CO6 storm outflows may partially explain the high ratios that were observed for these storms.

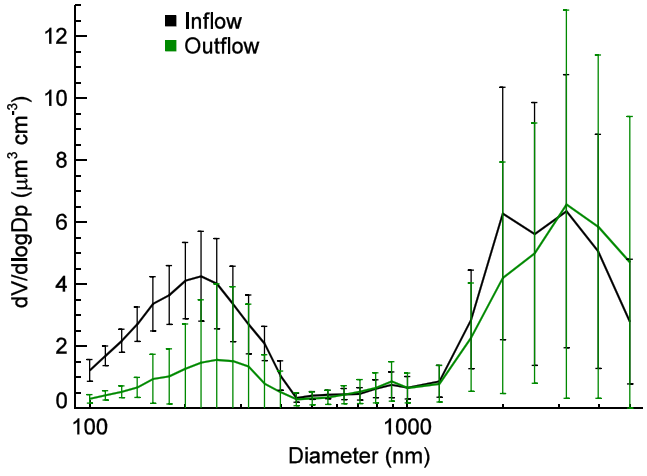

Figure 5. Inflow (black) and outflow (green) volume size distributions averaged for all storms. Inflow and outflow standard deviations are shown as black and green error bars, respectively. Volume size distributions were calculated from number size distributions measured by the LAS aboard the DC-8.

The storms sampled were far inland; thus, dust is expected to dominate the coarse-mode aerosol seen here. To examine this, regressions between Ca^{2+} mass concentrations and V_c averaged over each filter sampling period were performed (Figure 6). Ca^{2+} concentrations were not corrected for sea salt given the likely terrestrial source of Na^+ and Cl^- over the continental U.S. [*Pratt et al.*, 2010]. Correlation coefficients between V_c and Ca^{2+} concentrations are relatively high (>0.55) and statistically significant ($p < 0.005$). Thus, the coarse aerosol measured in storm outflow is assumed to be primarily dust. This is consistent with PALMS measurements

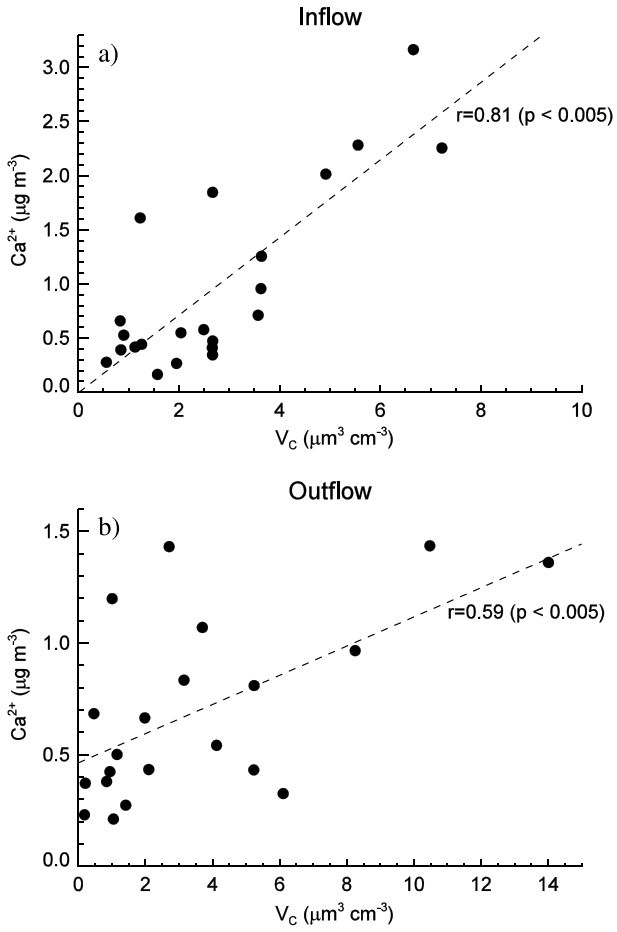

Figure 6. Ca^{2+} concentrations versus V_c for (a) inflow and (b) outflow filters. Linear regressions are shown as dashed line with statistically significant ($p < 0.005$) correlation coefficients. $Ca^{2+}$and V_c are reported in standard m^{-3} and standard cm^{-3}, respectively.

which, on average, identified 6 times as many dust particles compared to sea salt during the storm surveys (K. Froyd, personal communication, 2015).

4. Discussion

Mean inflow Ca^{2+} concentrations for all storms were generally higher than those measured in the lower free troposphere (<6 km) during other aircraft campaigns [e.g., *Talbot et al.*, 1998; *Avery et al.*, 2010]. For instance, *Talbot et al.* [1998] and *Tabazadeh et al.* [1998] report Ca^{2+} concentrations less than 1 $\mu g\,m^{-3}$ for altitudes less than 6 km in the region around the DOE ARM-CART site in OK, while DC3 inflow Ca^{2+} ranged from 0.39–2.71 $\mu g\,m^{-3}$ for all storms. The range of inflow Ca^{2+} concentrations shows more overlap with those measured in the tropics during the Tropical Composition, Clouds, and Climate Coupling experiment (TC^4) (0.08–1.34 $\mu g\,m^{-3}$) [*Avery et al.*, 2010]; however, mean inflow values during DC3 (1.20 ± 0.16 (1σ) $\mu g\,m^{-3}$) were larger than those seen during TC^4. The DC3 study region experienced a severe drought, and several wildfires occurred in New Mexico and Colorado during the DC3 sampling period (May/June 2012) [*Mallya et al.*, 2013; Huntrieser et al., submitted manuscript, 2015]; therefore, abnormally high concentrations of dust may have been available at the surface.

Ca^{2+} concentrations in storm outflow were an order of magnitude larger than mean free troposphere concentrations during DC3 (0.08 ± 0.06 (1σ) $\mu g\,m^{-3}$). Ca^{2+} enhancements in aged, cloud-free [*Liang et al.*, 2007] convective outflow as well as in the anvil region of tropical convective systems [*Avery et al.*, 2010] have been previously observed, though these outflow concentrations were generally lower than those reported here. For instance, *Liang et al.* [2007] reported Ca^{2+} concentrations associated with a cloud-free Asian plume transported via deep convection that were 5 times higher (0.20 $\mu g\,m^{-3}$) than their reported background concentrations (0.04 $\mu g\,m^{-3}$). *Avery et al.* [2010] also saw Ca^{2+} concentrations as high as 0.33 $\mu g\,m^{-3}$ between 10 and 11 km corresponding to convective outflow measured during TC^4, though it is possible this dust originated in the Saharan dust layer and not from the surface, given the sampling location. As mentioned above, inflow concentrations were generally higher than those measured previously at lower altitudes. Elevated inflow Ca^{2+} may therefore explain the higher mean outflow concentrations (0.66 ± 0.12 (1σ) $\mu g\,m^{-3}$) observed during DC3.

Such Ca^{2+} enhancements relative to background concentrations in storm outflow suggest convective systems represent an efficient mechanism to transport dust to the upper troposphere. High fractions of mineral dust particles identified by the PALMS in storm outflow during DC3 (K. Froyd, personal communication, 2015) and during TC^4 [*Froyd et al.*, 2009] further corroborate convective dust transport to the upper troposphere. Enhancements of coarse-mode aerosol in convective outflow were also observed recently during the Study of Emissions and Atmospheric Composition, Clouds, and Climate Coupling by Regional Surveys ($SEAC^4RS$) mission in August/September 2013 (Ziemba et al., submitted manuscript, 2015). Though a large fraction of the coarse-mode

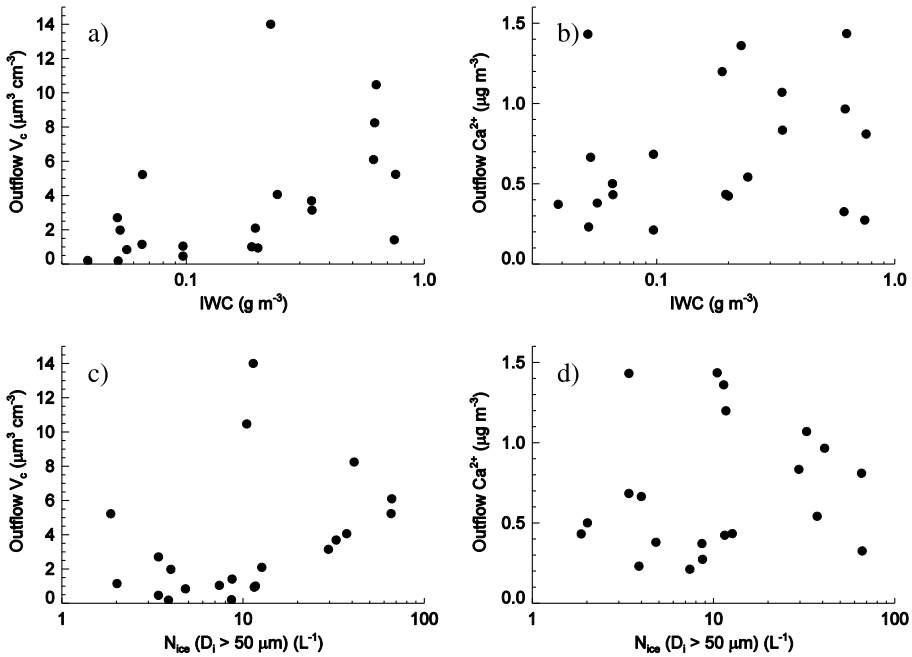

Figure 7. Mean IWC versus (a) mean outflow V_c and (b) mean outflow Ca^{2+} concentrations, and mean N_{ice} ($D_i > 50$ μm) versus (c) mean outflow V_c and (d) mean outflow Ca^{2+} concentrations for all storm filters.

particles measured during SEAC[4]RS contained a biological component, their presence further indicates coarse-mode aerosol can be efficiently transported through convective systems.

4.1. Influence of Ice Particles on Measurements

Recent research on the impact of ice crystals on airborne measurements in cirrus clouds indicate such measurements may be subject to contamination [e.g., *Murphy et al*., 2004; *Heymsfield*, 2007; *Jensen et al*., 2009; *Froyd et al*., 2010; *Lawson*, 2011; *Korolev et al*., 2013]. While much attention has been given to the impact of shattered ice on ice residual and ice concentration measurements, the aerosol composition and size measurements discussed here and those reported in previous work may also be subject to contamination by ice as suggested by recent airborne PALMS measurements [*Murphy et al*., 2004; *Froyd et al*., 2010; *Cziczo and Froyd*, 2014]. Specifically, several studies have noted a high (20–60%) proportion of single particle spectra collected by PALMS contained signatures of counterflow virtual impactor (CVI) inlet material (e.g., stainless steel) during in-cirrus sampling, implying ice impaction abrades the surface of CVI inlets [*Murphy et al*., 2004; *Froyd et al*., 2010; *Cziczo and Froyd*, 2014]. In addition to shredding inlet material, it is hypothesized that ice abrasion may also clean aerosol inlets of any accumulated particles, including coarse-mode dust. Assuming the inlets associated with the measurements discussed here are subject to the same ice artifacts as CVIs, ice impaction could result in erroneously high Ca^{2+} concentrations and V_c.

The aerosol artifact displays a noted size dependence, such that the inlet abrasion scales proportionally with the number of large ($D_i > 50$ μm) ice particles (N_{ice}) and IWC [*Froyd et al*., 2010]. As shown in Figure 7, there is no obvious dependence of outflow V_c nor outflow Ca^{2+} mass concentrations on either IWC or N_{ice}. Variations in the dust and V_c outflow/inflow ratios also appear independent of both ice parameters (Figure 8). In particular, those storms with V_c or dust ratios that exceed 1 occur over a range of N_{ice} and IWC values.

Because the bulk aerosol filters and LAS sample from independent inlets, ice abrasion would likely impact the two measurements differently. As discussed above and shown in Figure 6, statistically significant correlation coefficients are observed for both inflow and outflow. It should be noted that the slopes of the linear fits applied to the storm outflow data were different than those computed for the inflow, most likely due to the outflow V_c values that exceeded inflow values for some storms. While higher outflow V_c values may point to an inlet artifact associated with size distribution measurements, they more likely arise from the variability caused by the combination of long sampling time periods of the filter samples and the disconnect between

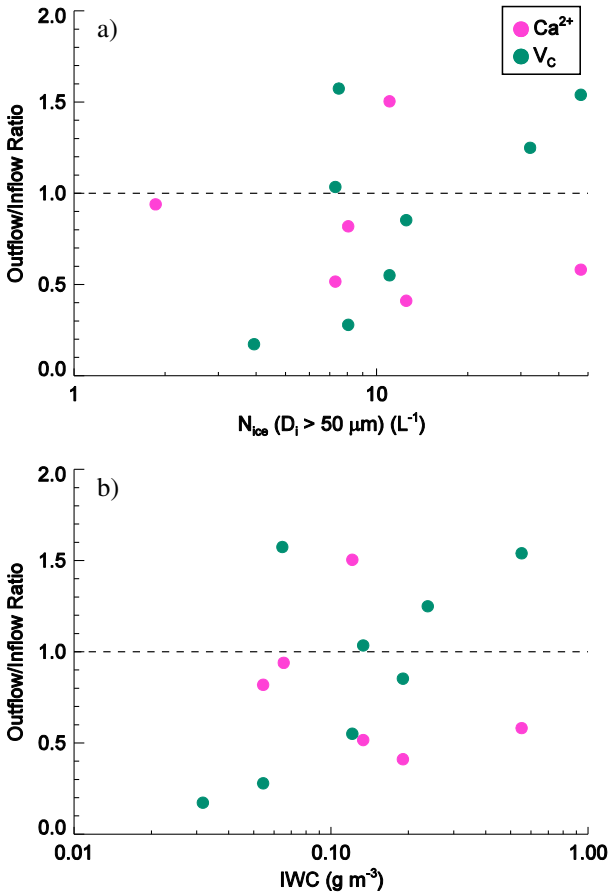

Figure 8. Storm outflow/inflow ratios for Ca^{2+} (pink) and V_c (green) versus (a) N_{ice} and (b) IWC. The dashed line denotes a ratio of 1.

inflow and outflow measurements due to the time it took the aircraft to reach the outflow after sampling the inflow region as suggested by Figure 8. Additionally, given the finite amount of dust deposited to the inlets, a decreasing trend in dust concentrations with time spent in the outflow would be expected if an abrasion artifact were present. However, this was not the case for the storms examined here, as demonstrated by the CO6 storm survey time series in Figure 1. This, together with the absence of a robust relationship between ice parameters and, V_c, Ca^{2+}, and outflow/inflow ratios, suggest inlet artifacts are small for the diffuser inlets used here.

4.2. Ice Nucleation Processes and Other Impacts on Scavenging During Vertical Transport

An explanation for the high transport efficiency of coarse dust through DC3 convective systems remains elusive at this time. At the very least, the results presented above indicate these very large particles are not efficiently removed by wet deposition, despite likely activating as cloud condensation nuclei (CCN) during transport through convective cells. Though identifying the reason for the apparent lack of warm-cloud scavenging in these storms is beyond the scope of this paper, two possible scenarios are proposed as follows: (1) the number of ambient dust particles that actually activate as CCN is small, allowing for the transport of dry dust to high altitudes or (2) activated dust particles are lofted to an altitude where the Wegener-Bergeron-Findeisen (WBF) process allows for the evaporation and release of dust back into the interstitial phase as ice particles grow at the expense of liquid cloud drops before the onset of precipitation. A comparison between maximum dust concentrations in liquid droplet residuals sampled in marine cumulus off the west coast of Africa during the NASA African Monsoon Multidisciplinary Analyses (NAMMA) (23–209 cm^{-3}) [*Twohy*, 2015] and average dust number concentrations in the Saharan Air Layer sampled during NAMMA (363 ± 78.2 cm^{-3}) [*Chen et al.*, 2011] suggests less than 60% of Saharan dust particles activate as CCN in tropical convection, though modeling work suggests this activated fraction increases with updraft velocity [*Twohy et al.*, 2009]. Alternatively, the WBF process has been used to explain the presence of interstitial coarse aerosol in stratiform mixed-phase clouds [e.g., *Henning et al.*, 2004; *Hoose et al.*, 2008]. *Korolev* [2006] suggests the WBF process may also occur in systems with median updraft velocities consistent with those observed for deep convective systems in the Central U.S. [*Giangrande et al.*, 2013], provided ice particle concentrations are sufficiently high. The WBF process was proposed to partially explain the presence of accumulation mode ($D_p > 0.12$ μm) aerosol near a tropical convective system above 9 km, though evaporation of activated aerosol as a result of entrainment and detrainment at the edges of the convective core also played a role [*Engstrom et al.*, 2008].

Because large ($D_p >$ ~0.5 μm) fresh mineral dust particles are relatively efficient IN [e.g., *Koehler et al.*, 2007; *DeMott et al.*, 2010; *Kanji et al.*, 2011; *Hoose and Mohler*, 2012; *DeMott et al.*, 2015], these particles would be

Table 3. Mean Inflow Aerosol Number Concentrations Calculated for an IN-Relevant Diameter Range ($0.5\,\mu m < D_p < 5\,\mu m$) ($N_{IN}$) and Mean Outflow Ice Particle Concentrations ($D_i > 10\,\mu m$)[a]

Storm	Inflow N_{IN} (L^{-1})	Outflow Ice Particle Concentration (L^{-1})
CO1	894 (1057)	40 (161)
CO2	1498 (3268)	7 (44)
CO3	1132 (985)	13 (95)
CO4	890 (866)	54 (218)
CO5	1916 (1555)	124 (620)
CO6	2003 (1448)	102 (349)
OK1	1347 (1118)	21 (109)
OK2	2932 (1688)	11 (30)
OK3	853 (944)	19 (74)

[a]1σ of inflow N_{IN} and the 95th percentile ice particle concentration values are shown in parentheses.

expected to initiate freezing once lofted to the WBF altitude. However, given the strong temperature and RH_i dependence of heterogeneous freezing mechanisms, the actual fraction of dust activated as IN is small. For instance, laboratory and field data show that less than 30% of the number of dust particles activate as IN during immersion freezing, the likely dominant freezing pathway in these systems given the probable activation of dust as CCN, even for temperatures as low as −35°C [*DeMott et al*., 2015]. Even smaller activation fractions may be expected depending on how quickly RH_i decreases below ice supersaturation during ice formation. While very low anvil temperatures (< −38°C) were observed for all storms, anvils were rarely at ice supersaturation [*Stith et al*., 2014]. Therefore, low activation fractions of dust are possible in these storm anvils.

To estimate the activated fraction of dust in the anvils of the nine DC3 storms investigated here, mean inflow proxy IN number concentrations (N_{PIN}), calculated as the sum of particles with diameters between 0.5 and 5 μm, were compared to mean outflow ice particle ($D_i > 10\,\mu m$) concentrations measured by the 2D-S (Table 3). This range is consistent with that discussed in *DeMott et al*. [2010] who saw a strong relationship between aerosol number concentrations for particles with diameters greater than 0.5 μm and IN concentrations. It should be noted that mean anvil ice concentrations may not be characteristic of the storm maximum ice particle concentrations and are only representative of the anvil at sampling time; significantly higher concentrations of ice particles have been observed in regions closer to storm updrafts and at younger anvil age [*Lawson et al*., 2010]. However, these presumed higher ice particle concentrations have previously been associated with homogeneous freezing and/or secondary ice particle formation rather than enhancements in IN activation [e.g., *Lawson et al*., 2010; *Gayet et al*., 2012; *Jensen et al*., 2013]. Therefore, comparisons between mean outflow ice concentrations and N_{PIN} provide a reasonable estimate of the IN efficiency of dust in these anvils.

Ice particle concentrations are a factor of ~15–300 times lower than N_{PIN} for all storms, indicating significantly more coarse-mode aerosol is ingested into these convective systems than has nucleated by the time it reaches the anvil (Table 3). Estimated interstitial N_{PIN} values, calculated as the difference between inflow N_{PIN} and outflow ice particle number concentrations, are comparable to mean inflow N_{PIN} (1496 ± 689 (1σ) L^{-1}) with a mean of 1453 L^{-1}. This is reflected in the interstitial N_{PIN}/inflow N_{PIN} ratios calculated for each storm which indicate, on average, less than 10% of the inflow dust particles act as IN during cirrus anvil formation. *Twohy* [2015] observed a similarly low fraction (0.1–10%) of ice residual dust for tropical convection influenced by the Saharan Air Layer. These high interstitial N_{PIN}/inflow N_{PIN} values are also consistent with the storm mean ratios calculated for Ca^{2+} (0.8 ± 0.40) and V_c (1.09 ± 0.75) and demonstrate that significant fractions of coarse-mode aerosol were transported through these DC3 systems. Ca^{2+} and V_c measured in convective outflow therefore likely represent interstitial coarse-mode dust.

5. Summary and Conclusions

Nine storms in the CO/OK region encountered by the NASA DC-8 aircraft during DC3 in May/June 2012 were used to investigate the convective transport of coarse-mode dust. Mass concentrations of bulk aerosol Ca^{2+} as well as total coarse (1 μm < diameter < 5 μm) aerosol volume (V_c) were higher than expected in the storm outflow region given that coarse mineral dust is likely to activate as CCN [*Twohy et al*., 2009; *Twohy*, 2015] and is a relatively efficient IN [e.g., *DeMott et al*., 2010; *Koehler et al*., 2010]. Comparisons between mean inflow and mean outflow concentrations indicate that less than ~50% of coarse-mode dust was scavenged by cloud

processes, which is substantially less than predicted by modeling studies [e.g., *Tulet et al.*, 2010]. However, the presence of elevated Ca^{2+} concentrations and V_c observed here are consistent with previous observations of enhancements in coarse-mode dust and dust tracers both in storm anvils and in cloud-free outflow air [e.g., *Liang et al.*, 2007; *Froyd et al.*, 2009; *Avery et al.*, 2010]. High fractions of interstitial dust may be possible even after activating as CCN if the WBF process is active in convective systems, as has been suggested by previous work [e.g., *Engström et al.*, 2008], and/or low fractions of dust activate as IN in the immersion mode, as observed in laboratory studies [e.g., *DeMott et al.*, 2015]; however, the details of these mechanisms remain poorly understood. Because coarse-mode dust is associated with significant indirect climate impacts [e.g., *Lohmann et al.*, 2008; *Lui et al.*, 2012], a better understanding of its transport to the upper troposphere is needed.

Artifacts associated with ice particles have recently been acknowledged for several ice particle concentration instruments [e.g., *Jensen et al.*, 2009; *Korolev et al.*, 2013] as well as single aerosol particle composition measurements [e.g., *Murphy et al.*, 2004; *Froyd et al.*, 2010; *Cziczo and Froyd*, 2014]. Though possible ice-related errors in the size distribution and bulk aerosol composition measurements used here have also been proposed, a clear relationship between V_c or dust concentrations and both IWC and large ($D_i > 50\ \mu m$) ice particle number (N_{ice}) was not evident. Regardless, potential relationships between ice crystal properties and inlet artifacts should be the subject of future work to improve confidence in interstitial aerosol measurements via comparisons between aerosol properties measured using traditional inlets to those measured using recently developed inlets designed to reduce shatter [e.g., *Craig et al.*, 2013; *Korolev et al.*, 2013]. Additionally, rinsing the aerosol inlets used here and analyzing the rinse solutions would provide an estimate for the amount, and composition, of material deposited to inlet surfaces during flight.

Comparisons between inflow total aerosol number concentrations calculated for a proxy IN range ($0.5\ \mu m <$ diameter $< 5\ \mu m$) (N_{PIN}) and ice particle concentrations ($D_i > 10\ \mu m$) were made to investigate the removal efficiency of coarse-mode dust during ice cloud formation. Consistent with outflow dust concentration measurements, this comparison indicated, on average, less than 10% of inflow coarse-mode particles were activated as anvil IN for all storms. Recent observations of ice residuals from tropical convection anvils showed similarly low fractions (0.1–10%) Saharan dust in the marine boundary layer were activated as IN in the anvil [*Twohy*, 2015]. The estimated large fractions of interstitial N_{PIN} together with the observed transport efficiencies of dust and V_c therefore suggest convective systems are an effective mechanism for the transport of dust to the upper troposphere.

Acknowledgments

Corr was supported by an appointment to the NASA Postdoctoral Program administered by Oak Ridge Associated Universities through a contract with NASA. NASA investigators acknowledge support from the Radiation Sciences Program headed by Hal Maring. The National Center for Atmospheric Research is sponsored by the National Science Foundation. We thank Tom Ryerson at NOAA for the use of his DC3 NO data and Karl Froyd for the DC3 PALMS data. Special thanks to the entire DC3 Science Team, especially the pilots and flight crews of the NASA DC-8 for their important contributions. All data used in this analysis are free and publicly available at DOI: 10.5067/Aircraft/DC3/DC8/Aerosol-TraceGas.

References

Avery, M., et al. (2010), Convective distribution of tropospheric ozone and tracers in the Central American ITCZ region: Evidence from observations during TC4, *J. Geophys. Res.*, *115*, D00J21, doi:10.1029/2009JD013450.

Barth, M. C., et al. (2015), The Deep Convective Clouds and Chemistry (DC3) field campaign, B, *Am. Meteorol. Soc.*, doi:10.1175/BAMS-D-13-00290.1.

Benas, N., N. Hatzianastassiou, C. Matsoukas, A. Fotiadi, N. Mihalopoulos, and I. Vardavas (2011), Aerosol shortwave direct radiative effect and forcing based on MODIS Level 2 data in the Eastern Mediterranean (Crete), *Atmos. Chem. Phys.*, *11*, 12,647–12,662.

Cai, Y., D. C. Montague, and T. Deshler (2011), Comparison of measured and calculated scattering from surface aerosols with an average, size-dependent, and time-dependent refractive index, *J. Geophys. Res.*, *116*, D02202, doi:10.1029/2010JD014607.

Chen, G., et al. (2011), Observations of Saharan dust microphysical and optical properties from the Eastern Atlantic during NAMMA airborne field campaign, *Atmos. Chem. Phys.*, *11*, 723–740.

Craig, L., A. Moharrieri, A. Schanot, D. C. Rogers, B. Anderson, and S. Dhaniyala (2013), Characterizations of cloud droplet shatter artifacts in two airborne aerosol inlets, *Aerosol Sci. Technol.*, *47*, 661–671.

Cziczo, D. J., and K. D. Froyd (2014), Sampling the composition of cirrus ice residuals, *Atmos. Res.*, *142*, 15–31, doi:10.1016/j.atmosres.2013.06.012.

Cziczo, D. J., K. D. Froyd, C. Hoose, E. J. Jensen, M. Diao, M. A. Zondlo, J. B. Smith, C. H. Twohy, and D. M. Murphy (2013), Clarifying the dominant sources and mechanisms of cirrus cloud formation, *Science*, *340*, 1320–1324.

DeMott, P. J., D. J. Cziczo, A. J. Prenni, D. M. Murphy, S. M. Kreidenweis, D. S. Thomson, R. Borys, and D. C. Rogers (2003a), Measurements of the concentration and composition of nuclei for cirrus formation, *Proc. Natl. Acad. Sci. U.S.A.*, *100*, 14,655–14,660.

DeMott, P. J., K. Sassen, M. R. Poellot, D. Baumgardner, D. C. Rogers, S. D. Brooks, A. J. Prenni, and S. M. Kreidenweis (2003b)., African dust aerosols as atmospheric ice nuclei, *Geophys. Res. Lett.*, *30*(14), 1732, doi:10.1029/2003GL017410.

DeMott, P. J., A. J. Prenni, X. Liu, S. M. Kreidenweis, M. D. Petters, C. H. Twohy, M. S. Richardson, T. Eidhammer, and D. C. Rogers (2010), Predicting global atmospheric ice nuclei distributions and their impacts on climate, *Proc. Natl. Acad. Sci. U.S.A.*, *107*, 11,217–11,222.

DeMott, P. J., et al. (2015), Integrating laboratory and field data to quantify the immersion freezing ice nucleation activity of mineral dust particles, *Atmos. Chem. Phys.*, *15*, 393–409.

Dibb, J. E., R. W. Talbot, E. M. Scheuer, G. Seid, M. A. Avery, and H. B. Singh (2003), Aerosol chemical composition in Asian continental outflow during the TRACE-P campaign: Comparison with PEM-West B, *J. Geophys. Res.*, *108*(D21), 8851, doi:10.1029/2002JD003111.

Engström, A., A. M. L. Ekman, R. Krejci, J. Ström, M. de Reus, and C. Wang (2008), Observational and modelling evidence of tropical deep convective clouds as a source of mid-tropospheric accumulation mode aerosols, *Geophys. Res. Lett.*, *35*, L23813, doi:10.1029/2008GL035817.

Fadnavis, S., K. Semeniuk, L. Pozzoli, M. G. Schultz, S. D. Ghude, S. Das, and R. Kakatkar (2013), Transport of aerosols into the UTLS and their impact on the Asian monsoon region as seen in a global model simulation, *Atmos. Chem. Phys.*, *13*, 8771–8786.
Froyd, K. D., D. M. Murphy, T. J. Sanford, D. S. Thomson, J. C. Wilson, L. Pfister, and L. Lait (2009), Aerosol composition of the tropical upper troposphere, *Atmos. Chem. Phys.*, *9*, 4363–4385.
Froyd, K. D., D. M. Murphy, P. Lawson, D. Baumgardner, and R. L. Herman (2010), Aerosols that form subvisible cirrus at the tropical tropopause, *Atmos. Chem. Phys.*, *10*, 209–218.
Fu, X., S. X. Wang, Z. Cheng, J. Xing, J. D. Zhao, and J. M. Hao (2014), Source, transport, and impacts of a heavy dust event in the Yangtze River Delta, China, in 2011, *Atmos. Chem. Phys.*, *14*, 1239–1254.
Gayet, J.-F., et al. (2012), On the observation of unusually high concentration of small chain-like aggregate crystals and large ice water content near the top of a deep convective cloud during the CIRCLE-2 experiment, *Atmos. Chem. Phys.*, *12*, 727–744.
Giangrande, S. E., S. Collis, J. Straka, A. Protat, C. Williams, and S. Krueger (2013), A summary of convective-core vertical velocity properties using ARM UHF wind profilers in Oklahoma, *J. Appl. Meteorol. Climatol.*, *52*, 2278–2295.
Henning, S., S. Bojinski, K. Diehl, S. Ghan, S. Nyeki, E. Weingartner, S. Wurzler, and U. Baltensperger (2004), Aerosol partitioning in natural mixed-phase clouds, *Geophys. Res. Lett.*, *31*, L06101, doi:10.1029/2003GL019025.
Herbert, R. J., B. J. Murray, S. J. Dobbie, and T. Koop (2015), Sensitivity of liquid clouds to homogeneous freezing parameterizations, *Geophys. Res. Lett.*, *42*, 1599–1605, doi:10.1002/2014GL062729.
Heymsfield, A. J. (2007), On measurements of small ice particles in clouds, *Geophys. Res. Lett.*, *24*, L23812, doi:10.1029/2007GL030951.
Homeyer, C. R., et al. (2014), Convective transport of water vapor into the lower stratosphere observed during double-tropopause events, *J. Geophys. Res. Atmos.*, *119*, doi:10.1002/2014JD021485.
Hoose, C., and O. Mohler (2012), Heterogeneous ice nucleation on atmospheric aerosols: A review of results from laboratory experiments, *Atmos. Chem. Phys.*, *12*, 9817–9854.
Hoose, C., U. Lohmann, P. Stier, B. Verheggen, and E. Weingartner (2008), Aerosol processing in mixed-phase clouds in ECHAM5-HAM: Model description and comparison to observations, *J. Geophys. Res.*, *113*, D07210, doi:10.1029/2007JD009251.
Huntrieser, H., H. Schlager, C. Feigl, and H. Holler (1998), Transport and production of NO_x in electrified thunderstorms: Survey of previous studies and new observations at midlatitudes, *J. Geophys. Res.*, *103*, 28,247–28,264, doi:10.1029/98JD02353.
Jensen, E. J., et al. (2009), On the importance of small ice crystals in tropical anvil cirrus, *Atmos. Chem. Phys.*, *9*, 5519–5537.
Jensen, E. J., R. P. Lawson, J. W. Bergman, L. Pfister, T. P. Bui, and C. G. Schmitt (2013), Physical processes controlling ice concentrations in synoptically forced, midlatitude cirrus, *J. Geophys. Res. Atmos.*, *118*, 5348–5360, doi:10.1002/jgrd.50421.
Jickells, T. D., et al. (2005), Global iron connections between desert dust, ocean biogeochemistry, and climate, *Science*, *308*, 67–71.
Kanji, Z. A., P. J. DeMott, O. Mohler, and J. P. D. Abbatt (2011), Results from the University of Toronto continuous flow diffusion chamber, at ICIS 2007: Instrument intercomparison and ice onsets for different aerosol types, *Atmos. Chem. Phys.*, *11*, 31–41.
Kline, J., B. Huebert, S. Howell, B. Blomquist, J. Zhuang, T. Betram, and J. Carrillo (2004), Aerosol composition and size versus altitude measured from the C-130 during AC-Asia, *J. Geophys. Res.*, *109*, D19S08, doi:10.1029/2004JD004540.
Koehler, K. A., S. M. Kreidenweis, P. J. DeMott, A. J. Prenni, and M. D. Petters (2007), Potential impact of Owens (dry) Lake dust on warm and cold cloud formation, *J. Geophys. Res.*, *112*, D12210, doi:10.1029/2007JD008413.
Koehler, K. A., S. M. Kreidenweis, P. J. DeMott, M. D. Petters, A. J. Prenni, and O. Mohler (2010), Laboratory investigations of the impact of mineral dust aerosol on cold cloud formation, *Atmos. Chem. Phys.*, *10*, 11,955–11,968.
Korolev, A. (2006), Limitation of the Wegner-Bergeron-Findeisen mechanism in the evolution of mixed-phase clouds, *J. Atmos. Sci.*, *64*, 3372–3375.
Korolev, A. V., E. F. Emery, J. W. Strapp, S. G. Cober, and G. A. Isaac (2013), Quantification of the effects of shattering on airborne ice particle measurements, *J. Atmos. Oceanic Technol.*, *30*, 2527–2553.
Lawson, R. P. (2011), Effects of ice particles shattering on the 2D-S probe, *Atmos. Meas. Tech*, *4*, 1361–1381.
Lawson, R. P., D. O'Connor, P. Zmarzly, K. Weaver, B. Baker, and Q. Mo (2006), The 2D-S (Stereo) probe: Design and preliminary tests of a new airborne, high-speed, high-resolution particle imaging probe, *J. Atmos. Oceanic Technol.*, *23*, 1462–1477.
Lawson, R. P., E. Jensen, D. L. Mitchell, B. Baker, Q. Mo, and B. Pilson (2010), Microphysical and radiative properties of tropical clouds investigated in TC4 and NAMMA, *J. Geophys. Res.*, *115*, doi:10.1029/2009JD013017.
Liang, Q., et al. (2007), Summertime influence of Asian pollution in the free troposphere over North America, *J. Geophys. Res.*, *112*, doi:10.1029/2006JD007919.
Lohmann, U., P. Spichtinger, S. Jess, T. Peter, and H. Smit (2008), Cirrus cloud formation and ice supersaturated regions in a global climate model, *Environ. Res. Lett.*, *3*, doi:10.1088/1748-9326/3/4/045022.
Lui, X., X. Shi, K. Zhang, E. J. Jensen, A. Gettelman, D. Barahona, A. Nenes, and P. Lawson (2012), Sensitivity studies of dust ice nuclei effects on cirrus clouds with the Community Atmosphere Model (CAM5), *Atmos. Chem. Phys.*, *12*, 12,061–12,079.
Mallya, G., L. Zhao, X. C. Song, D. Niyogi, and R. S. Govindaraju (2013), 2012 Midwest drought in the United States, *J. Hydrol. Eng.*, *18*, 737–745.
Malm, W. C., B. A. Schichtel, M. L. Pitchford, L. L. Ashbaugh, and R. A. Eldred (2004), Spatial and monthly trends in speciated fine particle concentration in the United States, *J. Geophys. Res.*, *109*, D03306, doi:10.1029/2003JD003739.
McNaughton, C. S., et al. (2007), Results from the DC-8 inlet characterization experiment (DICE): Airborne versus surface sampling of mineral dust and sea salt aerosols, *Aerosol Sci. Technol.*, *41*, 136–159.
Murphy, D. M., D. J. Cziczo, P. K. Hudson, D. S. Thomson, J. C. Wilson, T. Kojima, and P. R. Buseck (2004), Particle generation and resuspension in aircraft inlets when flying in clouds, *Aerosol Sci. Technol.*, *38*, 401–409, doi:10.1080/02786820490443094.
Murphy, D. M., D. J. Cziczo, K. D. Froyd, P. K. Hudson, B. M. Matthew, A. M. Middlebrook, R. E. Peltier, A. Sullivan, D. S. Thomson, and R. J. Weber (2006), Single-particle mass spectrometry of tropospheric aerosols, *J. Geophys. Res.*, *111*, D23S32, doi:10.1029/2006JD007340.
Pratt, K. A., et al. (2010), Observation of playa salts as nuclei in orographic wave clouds, *J. Geophys. Res.*, *115*, D15301, doi:10.1029/2009JD013606.
Prospero, J. M., and T. N. Carlson (1972), Vertical and areal distributions of Saharan dust over the western equatorial North Atlantic Ocean, *J. Geophys. Res.*, *77*, 5255–5265, doi:10.1029/JC077i027p05255.
Querol, X., et al. (2008), Spatial and temporal variations in airborne particulate matter (PM_{10} and $PM_{2.5}$) across Spain 1999–2005, *Atmos. Environ.*, *42*, 3964–3979.
Richardson, M. S., et al. (2007), Measurements of heterogeneous ice nuclei in the western United States in springtime and their relation to aerosol characteristics, *J. Geophys. Res.*, *112*, D02209, doi:10.1029/2006JD007500.
Ryder, C. L., et al. (2013), Optical properties of Saharan dust aerosol and contribution from the coarse mode as measured during the Fennec 2011 aircraft campaign, *Atmos. Chem. Phys.*, *13*, 303–325.
Ryerson, T. B., L. G. Huey, K. Knapp, J. A. Neuman, D. D. Parrish, D. T. Sueper, and F. C. Fehsenfeld (1999), Design and initial characterization of an inlet for gas-phase NO_y measurements from aircraft, *J. Geophys. Res.*, *104*, 5483–5492, doi:10.1029/1998JD100087.

Scheuer, E., J. E. Dibb, C. Twohy, D. C. Rogers, A. J. Heymsfield, and A. Bansemer (2010), Evidence of nitric acid uptake in warm cirrus anvil clouds during the NASA TC4 campaign, *J. Geophys. Res.*, *115*, D00J03, doi:10.1029/2009JD012716.

Schroeder, J. R. (2015), Analysis of the effects of midlatitude deep convection on the composition and chemistry of the upper troposphere/lower stratosphere using airborne measurements of VOCs and other trace gases, PhD dissertation, pp. 65–86, Univ. of Calif., Irvine.

Schroeder, J. R., L. L. Pan, T. Ryerson, G. Diskin, J. Hair, S. Meinardi, I. Simpson, B. Barletta, N. Blake, and D. R. Blake (2014), Evidence of mixing between polluted convective outflow and stratospheric air in the upper troposphere during DC3, *J. Geophys. Res. Atmos.*, *119*, 11,477–11,491, doi:10.1002/2014JD022109.

Schumann, U., and H. Huntrieser (2007), The global lightning-induced nitrogen oxides source, *Atmos. Chem. Phys.*, *7*, 3823–3907.

Seigel, R. B., and S. C. van den Heever (2012), Dust lofting and ingestion by supercell storms, *J. Atmos. Sci.*, *69*, 1453–1473.

Skamarock, W. C., J. G. Powers, M. Barth, J. E. Dye, T. Matejka, D. Bartels, K. Baumann, J. Stith, D. D. Parrish, and G. Hubler (2000), Numerical simulations of the July 10 stratospheric-tropospheric experiment: Radiation, aerosols, and ozone/deep convection experiment convective systems: Kinematics and transport, *J. Geophys. Res.*, *105*(D15), 19,973–19,990, doi:10.1029/2000JD900179.

Stith, J. L., L. M. Avallone, A. Bansemer, B. Basarab, S. W. Dorsi, B. Fuchs, R. P. Lawson, D. C. Rogers, S. Rutledge, and D. W. Toohey (2014), Ice particles in the upper anvil regions of midlatitude continental thunderstorms: The case for frozen-drop aggregates, *Atmos. Chem. Phys.*, *14*, 1973–1985.

Tabazadeh, A., M. Z. Jacobson, H. B. Singh, O. B. Toon, J. S. Lin, B. Chatfield, A. N. Thakur, R. W. Talbot, and J. E. Dibb (1998), Nitric acid scavenging by mineral and biomass aerosols, *Geophys. Res. Lett.*, *25*, 4185–4188, doi:10.1029/1998GL900062.

Takemi, T., M. Yasui, J. Zhou, and L. Liu (2006), Role of boundary layer and cumulus convection on dust emission and transport over a midlatitude desert area, *J. Geophys. Res.*, *111*, D11203, doi:10.1029/2005JD006666.

Talbot, R. W., J. E. Dibb, and M. B. Loomis (1998), Influence of vertical transport on free tropospheric aerosols over the central USA in springtime, *Geophys. Res. Lett.*, *25*, 1367–1370, doi:10.1029/98GL00184.

Thornhill, K. L., et al. (2008), The impact of local sources and long-range transport on aerosol properties over the northeast U.S. region during INTEX-NA, *J. Geophys. Res.*, *113*, D08201, doi:10.1029/2007JD008666.

Tsamalis, C., A. Chedin, J. Pelon, and V. Capelle (2013), The seasonal vertical distribution of the Saharan Air Layer and its modulation by the wind, *Atmos. Chem. Phys.*, *13*, 11,235–11,257.

Tulet, P., K. Crahan-Kaku, M. Leriche, B. Aouizerats, and S. Crumeyolle (2010), Mixing of dust aerosols into a mesoscale convection system: Generation, filter and possible feedback on ice anvils, *Atmos. Res.*, *9*, 302–314.

Twohy, C. H. (2015), Measurements of Saharan dust in convective clouds over tropical eastern Atlantic Ocean, *J. Atmos. Sci.*, *72*, 75–81.

Twohy, C. H., et al. (2009), Saharan dust particles nucleate droplets in eastern Atlantic clouds, *Geophys. Res. Lett.*, *36*, L01807, doi:10.1029/2008GL035846.

Yin, Y., Q. Chen, L. Jin, B. Chen, S. Zhu, and X. Zhang (2012), The effects of deep convection on the concentration and size distribution of aerosol particles within the upper troposphere: A case study, *J. Geophys. Res.*, *117*, D22202, doi:10.1029/2012JD017827.

Zhang, X. Y., Y. Q. Wang, T. Niu, X. C. Zhang, S. L. Gong, Y. M. Zhang, and J. Y. Sun (2012), Atmospheric aerosol compositions in China: Spatial/temporal variability, chemical signatures, regional haze distribution and comparison with global aerosols, *Atmos. Chem. Phys.*, *12*, 779–799.